Journal of Proteomics 149 (2016) 53–63

Contents lists available at ScienceDirect

Journal of Proteomics

journal homepage: www.elsevier.com/locate/jprot

Proteomic changes in human lung epithelial cells (A549) in response to carbon black and titanium dioxide exposures

Ngoc Q. Vuong [a,d], Patrick Goegan [a], Susantha Mohottalage [b], Dalibor Breznan [a], Marianne Ariganello [a], Andrew Williams [c], Fred Elisma [b], Subramanian Karthikeyan [a], Renaud Vincent [a,d], Premkumari Kumarathasan [b,*]

[a] Inhalation Toxicology Laboratory, Environmental Health Science and Research Bureau, Health Canada, Ottawa, ON K1A 0K9, Canada
[b] Analytical Biochemistry and Proteomics, Environmental Health Science and Research Bureau, Health Canada, Ottawa, ON K1A 0K9, Canada
[c] Biostatistics Section, Population Studies Division, Environmental Health Science and Research Bureau, Health Canada, Ottawa, ON K1A 0K9, Canada
[d] Department of Biochemistry, Faculty of Science, University of Ottawa, Ottawa, ON K1H 8M5, Canada

ARTICLE INFO

Article history:
Received 1 December 2015
Received in revised form 12 March 2016
Accepted 26 March 2016
Available online 12 April 2016

Keywords:
Titanium dioxide
Carbon black
A549
Toxicoproteomics
Cytotoxicity assay
2D-GE

ABSTRACT

This study combined cytotoxicity assays with proteomic analysis to characterize the unique biological responses of the A549 human lung epithelial cell line to two physicochemically distinct respirable particles titanium dioxide (TiO_2) and carbon black (CB). Cellular LDH, ATP, BrdU incorporation and resazurin reduction indicated that CB was more potent than TiO_2. Proteomic analysis was done using 2D-GE and MALDI-TOF-TOF-MS. Proteomic changes reflected common and particle-specific responses. Particle-specific proteomic responses were associated with cell death (necrosis and apoptosis), viability and proliferation pathways. Our results suggested that these pathways were consistent with the cytotoxicity data. For instance, increased expressions of anti-proliferative proteins LMNA and PA2G4 were in agreement with the decreased BrdU incorporation in A549 cells after exposure to CB. Similarly, increased expression of HSPA5 that is associated with ATPase activity was consistent with decreased cellular ATP levels in these cells. These findings reveal that proteomic changes can explain the cellular cytotoxicity characteristics of the particles. In essence, our results demonstrate that the *in vitro* toxicoproteomic approach is a promising tool to gain insight into molecular mechanisms underlying particle exposure-specific cytotoxicity.

Biological significance: In this study we have shown that toxicoproteomics is a sensitive and informative method to resolve the toxicity characteristics of particles with different physicochemical properties. This approach can be useful in the investigation of molecular mechanisms underpinning cellular cytotoxic responses elicited by particle exposures. Thus, the toxicoproteomic approach can be valuable in assessing the risk associated with particle exposures *in vitro*.

1. Introduction

Airborne particulate matter (PM) is a complex mixture of inorganic and organic compounds. Inhalation of airborne PM has been linked to the development or exacerbation of respiratory illnesses such as bronchitis [1–3], asthma [4–6], cystic fibrosis [7,8] and lung cancer [2,9–12].Toxicity of urban air particles and their associated adverse health outcomes can vary with particle composition. Insight into particle exposure-specific molecular mechanisms can provide a biological basis of particle toxicity. In this study, we focused on an *in vitro* toxicoproteomic approach that can distinguish the toxic effects of two particles that are chemically and physically different.

Carbon black (CB) is a manufactured product containing predominantly (95%) elemental carbon (EC) with negligible amounts of inorganic and organic materials [13,14] and should not be confused with black carbon (soot) that contains varying amounts of EC, organic materials and metals [14,15]. Recent reports have implied that exposure to elemental carbon (EC) can have a negative impact on the cardiovascular system [16–19]. Yet, toxicity mechanisms underpinning EC exposure-related adverse cardiovascular effects are not clear, and CB has been used as a surrogate for EC in *in vitro* and *in vivo* toxicity studies [20–25]. Meanwhile, titanium dioxide (TiO_2) is typically used as a "negative control" in many particle toxicology studies due to its relative low toxicity properties both *in vivo* and *in vitro*. Nevertheless, recent studies have reported that the toxicity of TiO_2 could depend on

* Corresponding author at: 0803C Tunney's Pasture, Ottawa, ON, Canada.
E-mail address: premkumari.kumarathasan@canada.ca (P. Kumarathasan).

http://dx.doi.org/10.1016/j.jprot.2016.03.046

physicochemical parameters such as size, aggregation, crystal phase and surface modifications [26].

Cytotoxicity of particles has traditionally been assessed by endpoint assays such as resazurin reduction, cellular ATP, lactate dehydrogenase (LDH) release and 5-bromo-2′-deoxyuridine (BrdU) incorporation. These assays are attractive to researchers because they can be applied in a high-throughput manner to estimate the toxic potency of respirable particles. One of the drawbacks of these cytotoxic assays is that they do not reveal detailed information at the molecular level. In recent years, proteomic-based approaches have gained momentum in toxicology based on their ability to delineate the molecular mechanism underlying the toxicity of PM [27,28]. Protein separation by two-dimensional gel electrophoresis (2D-GE) followed by protein identification by mass spectrometry (MS) or tandem mass spectrometry (MS/MS) is a classical proteomic approach used to quantify and identify proteins in complex biological matrices. While shot-gun proteomic analyses (using MALDI-TOF-TOF/MS/MS or LC/MS/MS) are proposed alternatives to gel-based proteomic procedures, the advantage of 2D-GE is that it is relatively inexpensive and can provide high content data. Recent studies have used 2D-GE to identify proteomic changes in cells to help characterize the toxicity caused by exposure to particles [27,29–34].

In this study, in order to understand particle-specific cellular changes we exposed a human lung epithelial cell line (A549) to two chemically and physically different respirable materials, CB and TiO_2 particle. We then used a toxicoproteomic approach by conducting traditional cytotoxicity assays along with proteomics to identify the molecular signature of particle toxicity.

2. Materials and methods

2.1. Materials

Culture flasks (T-25 and T-75), 96-well plate and plastic cell scrapers were obtained from Corning Inc. (Corning, NY). Dulbecco's Modified Eagle's Medium (DMEM) and fetal bovine serum (FBS) were purchased from HyClone (Logan, UT). Gentamicin, trifluoroacetic acid, α-cyano-4-hydroxy-cinnamic acid, Tris-HCl, NaCl, Tween-20 and Tween-80 were obtained from Sigma-Aldrich (Oakville, ON). Iodoacetamide, bis-acrylamide, ammonium persulfate, glycerol, immobilized pH gradient strips, Criterion Cassette (13.3 × 8.7 cm W × L), Tris/Glycine/SDS buffer, and BioSafe Coomassie Blue were purchased from Bio-Rad (Mississauga, ON). Trypsin, resazurin reduction (CellTiter-Blue®) and lactate dehydrogenase (LDH) cytotoxicity assay kits (CytoTox-96®) were from Promega Corporation (Madison, WI), ATP assay kit (ViaLight™ Plus) was purchased from Lonza Corporation (Rockland, ME), and 5-bromo-2′-deoxyuridine (BrdU) cell proliferation ELISA (chemiluminescent) assay kit was obtained from Roche Diagnostics (Laval, QC). All water used was deionized/demineralized (>16 MΩ resistivity).

2.2. Particles preparation

TiO_2 (SRM-154b) obtained from the National Institute of Standards and Technology (Gaithersburg, MD) was subjected to three successive washes with methanol and then phosphate buffered saline (PBS) to remove possible soluble metals and organic contaminants before use in the experiments [35]. Carbon black (Cas#1333-86-4) obtained from Cabot Corporation (Boston, MA) was used as received. Particles were resuspended at 10 mg/mL in particle buffer (0.19% NaCl and 25 μg/mL Tween-80) [36], vortexed (30 s), sonicated (20 min on ice), homogenized with a Dounce Homogenizer (25 strokes), and then heated (56 °C, 1 h). The particles were stored at −40 °C until use.

2.3. Cell culture and particle exposure

The A549 cell line (American Type Culture Collection - CCL-185; human, epithelial, lung carcinoma) was subcultured in DMEM supplemented with 50 μg/mL gentamycin and 10% FBS. The cells were maintained in T-75 flasks in a humidified atmosphere at 37 °C containing 5% CO_2 and 95% air. For experiments, the cells were seeded at 1.5×10^6 cells (T-25), 3.75×10^6 cells (T-75) or 2.0×10^4 cells/well (96-well plate for cytotoxicity assays) and incubated for 24 h, resulting in approximately 75% confluence prior to dosing with particles. The final volume of culture medium was 5 mL (T-25), 15 mL (T-75) or 200 μL/well (96-well plate). Solutions of particles were prepared by thawing the frozen stocks to aqueous solutions, sonicating on ice (20 min) then diluting in the culture medium to make up dosing concentrations of 0, 60, 140 and 200 μg/cm^2. The cells were exposed to the particles by replacing the existing culture medium with the particle solutions, and the flasks/plates were returned to the incubator and allowed to incubate for 24 h. To harvest the exposed cells, the medium in each flask was removed and the cells were detached from the flasks using a plastic scraper. The cell suspension was collected in cell culture medium and centrifuged at 350 ×*g* for 5 min, and the supernatant was removed. The cell pellet was then washed twice with PBS. The final cell pellet was aspirated dry and stored frozen at −80 °C until further use. The integrated cytotoxicity bioassay which combined endpoints of cell viability (resazurin reduction assay), cellular membrane integrity (intracellular LDH content) and energy metabolism (ATP assay) were conducted in 96-well plates as described in our previous study [37]. The cell proliferation (BrdU incorporation) assay was conducted in a separate 96-well plate.

2.4. Protein extraction

The cell pellets were solubilized in a protein extraction/rehydration buffer from Bio-Rad (8 M urea, 2% CHAPS, 50 mM dithiothreitol, 0.2% Biolyte 3/10), where the volume depends on the number of cells in the pellet to achieve 1–2 μg/μL, and 1×10^6 A549 cells was experimentally estimated to yield about 200 μg of protein. The samples were vortexed (30 s), sonicated (10 min), vortexed (30 s) and centrifuged (15,000 ×*g*, 10 min). The extracted protein in the supernatant was collected, and the concentration of protein in each extract was determined immediately using the Coomassie Plus Protein assay kit (Thermo Scientific). The extracted protein samples were stored at −80 °C until use.

2.5. Two-dimensional gel electrophoresis (2D-GE)

2D-GE was conducted as described in our previous study [38]. Briefly, an appropriate quantity of protein was suspended in a total volume of 200 μL of extraction buffer, and applied to an immobilized pH gradient (IPG) strips (11 cm, pH 3–10 or pH 5–8) in a clean disposable rehydration tray and allowed to incubate for 1 h at room temperature. The IPG strip was then overlaid with mineral oil and allowed to continue incubating overnight (16–20 h). The IPG strip was then moved to an isoelectric focusing tray, overlaid with mineral oil and subjected to isoelectric focusing using a PROTEAN IEF cell (BioRad). The focusing conditions were as follows: stage 1: linear ramp to 250 V for 20 min; stage 2: linear ramp to 8000 V for 2.5 h; stage 3: rapid ramp for 20,000 V h. The strip was then stored at −80 °C until use. The focused IPG strip was thawed and gently agitated for 10 min in equilibration buffer 1 (6 M urea, 2% SDS, 375 mM Tris-HCl, 20% glycerol, 130 mM dithiothreitol, 0.001% bromophenol blue). Then each strip was gently agitated for another 10 min in equilibration buffer 2 (6 M urea, 2% SDS, 375 mM Tris-HCl, 20% glycerol, 135 mM iodoacetamide, 0.001% bromophenol blue). The strip was then placed on a 12% SDS-PAGE gel casted in a 1.0 mm thick Criterion Cassette (13.3 × 8.7 cm W × L) and subjected to electrophoresis at 200 V for 65 min. Following electrophoresis, the gel was removed from the Criterion Cassette, washed for 30 min in water, stained in BioSafe Coomassie Blue (Bio-Rad) overnight (16–20 h), destained twice in water, and then imaged with a standard scanner.

To overcome the typical warping and distortion issues from gel to gel near the extremities of the pH and the molecular weight range, a

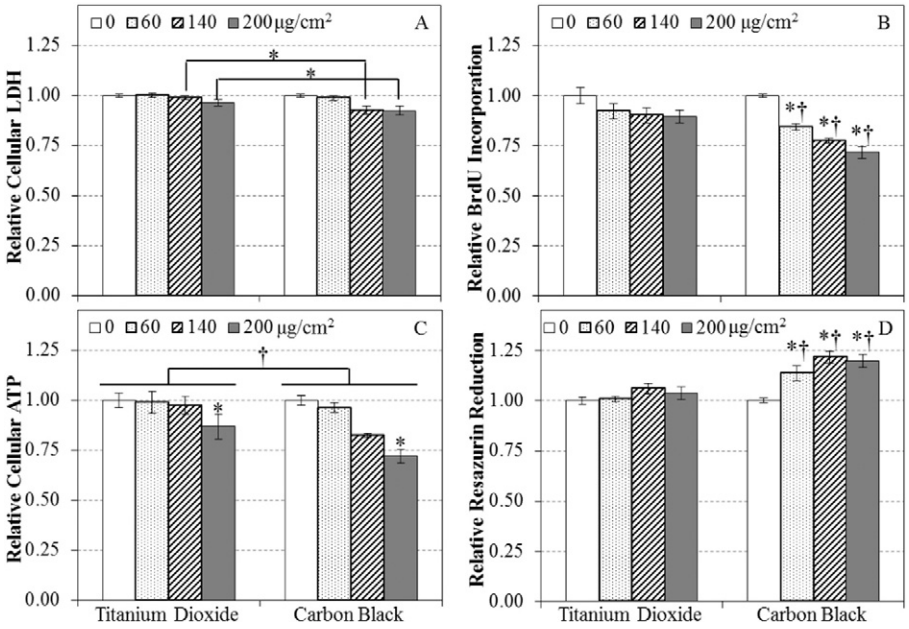

Fig. 1. The cytotoxicity of titanium dioxide and carbon black in A549 cells after 24 h of exposure were examined by cellular LDH (A), BrdU incorporation (B), cellular ATP (C) and resazurin reduction (D) assays. Data are expressed as mean fold effect ± standard error, relative to control (0 µg/cm^2), n = 4. Two-way ANOVA was used to determine significant effects of the particles, where Holm-Sidak was the post-hoc method used for all pairwise comparison procedures. * indicates a significant change ($p < 0.05$) compared to control (0 µg/cm^2) and † indicates significant differences between the two particles.

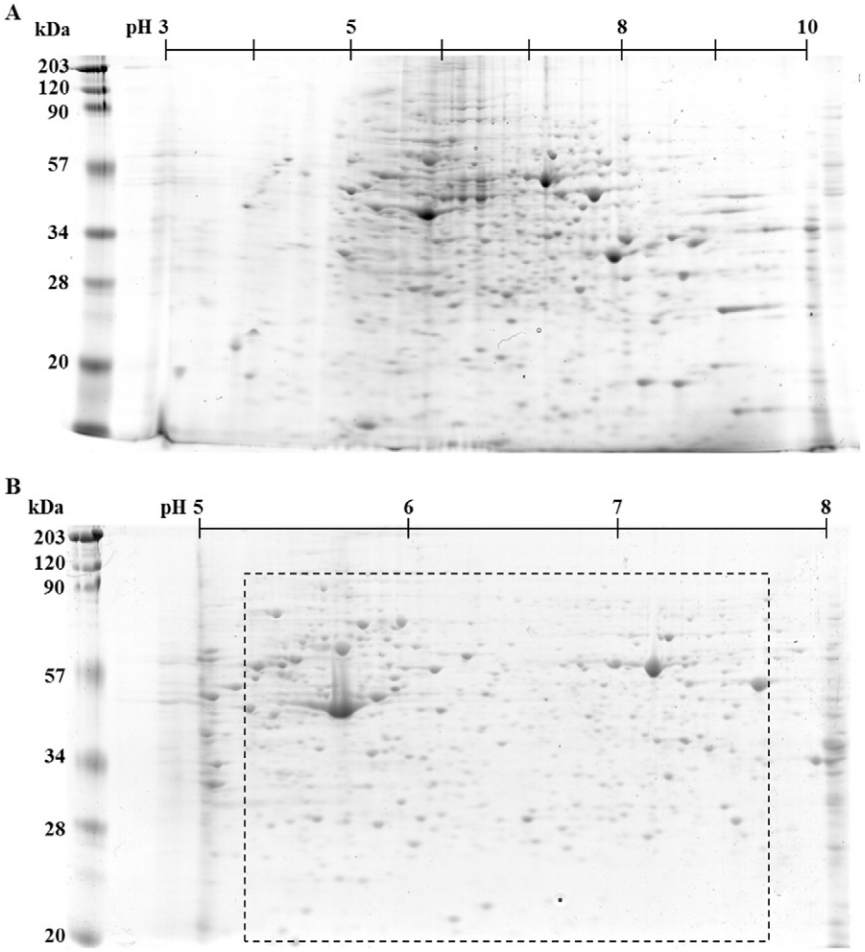

Fig. 2. Selection of the information-rich region in the two-dimensional gel electrophoresis (2D-GE) map of A549 proteins to investigate particle exposure-related changes.

common area (Fig. 2; pH 5.1–7.8 and 100–20 kDa) that clearly shows the protein spots across all experimental gels was selected to assess the proteome differences among the treatments. The protein spots within the gels were matched and quantified with PDQuest™ Advance V8.0.1 (Bio-Rad), where spot volume was quantified using the available "Local regression model (LOESS)" algorithm in PDQuest. The reported normalized spot volume for each protein was used to compare its level of expression across the treatments. Three gels representing three biological repeats were generated for each group in this experiment to assess the particle-induced changes in the proteome of A549 cells.

2.6. In-gel digest, preparing protein spots for identification

To identify the protein in each spot of interest, a large set of preparative gels (10–12 gels) were prepared with 175 μg of protein/gel as described above. The gels were then stained with Biosafe Coomassie blue and imaged. The spots in preparative gels were then aligned and matched to the experimental gels using PDQuest. The protein spots were then excised from the preparative gels with an automated spot cutter equipped with a 1.5 mm cutting head (ExQuest from Bio-Rad). The excised gels corresponding to the same protein spot from different preparative gels were pooled into the same tube for maximum protein yield. The excised gels were then subjected to in-gel tryptic digest as described in our previous study [38]. Briefly, the gel spots were destained and then subjected to a 16 h digestion by trypsin (pH = 7) at 37 °C. All the digested samples were evaporated under a gentle stream of N_2(g) and were stored at −80 °C until further use.

2.7. Matrix-assisted laser desorption/ionization time-of-flight mass spectrometry (MALDI-TOF-TOF-MS)

Each sample was reconstituted in 5 to 20 μL of 30% acetonitrile (ACN) in 0.1% trifluoroacetic acid (TFA) depending on the spot volume and was spotted (1.5 μL) on an AnchorChip target plate (600/384F, Bruker Daltonics Ltd, Bremen, Germany) together with 1.5 μL of freshly prepared α-cyano-4-hydroxy-cinnamic acid (5 μg/μL in 50% ACN in 0.1% TFA). The spotted sample/matrix was dried under vacuum for at least 2 h. Each dried sample/matrix was washed with 2.5 μL of cold 0.1% TFA and briefly dried under vacuum. Each sample was analyzed by MALDI-TOF-TOF-MS using an automated analysis option (Bruker Daltonics, Bremen, Germany). In brief, MS scan of each spot was done to obtain the peptide mass fingerprint (PMF). Six major analyte peaks from the PMF spectrum were subjected to tandem MS (MS/MS) analysis in the "voltage lift mode". The mass spectral information was matched against the SwissProt and RefSeq data bases using the Mascot search engine (Matrix Sciences) for protein identification. In the case that >1 protein was identified per spot, we attributed the protein with the highest score to such spot.

2.8. Statistics and bioinformatics

Two-way analysis of variance (ANOVA) was performed on 2D-GE and cytotoxicity (LDH, BrdU, ATP and CTB) data with treatment and dose as factors. When the assumption of equal variance and normal distribution were not met, the data were rank-transformed. Holm-Sidak was the post-hoc method used for all pairwise comparison procedures. A data point is considered as significant if $p < 0.05$. If the *Treatment* x *Dose*

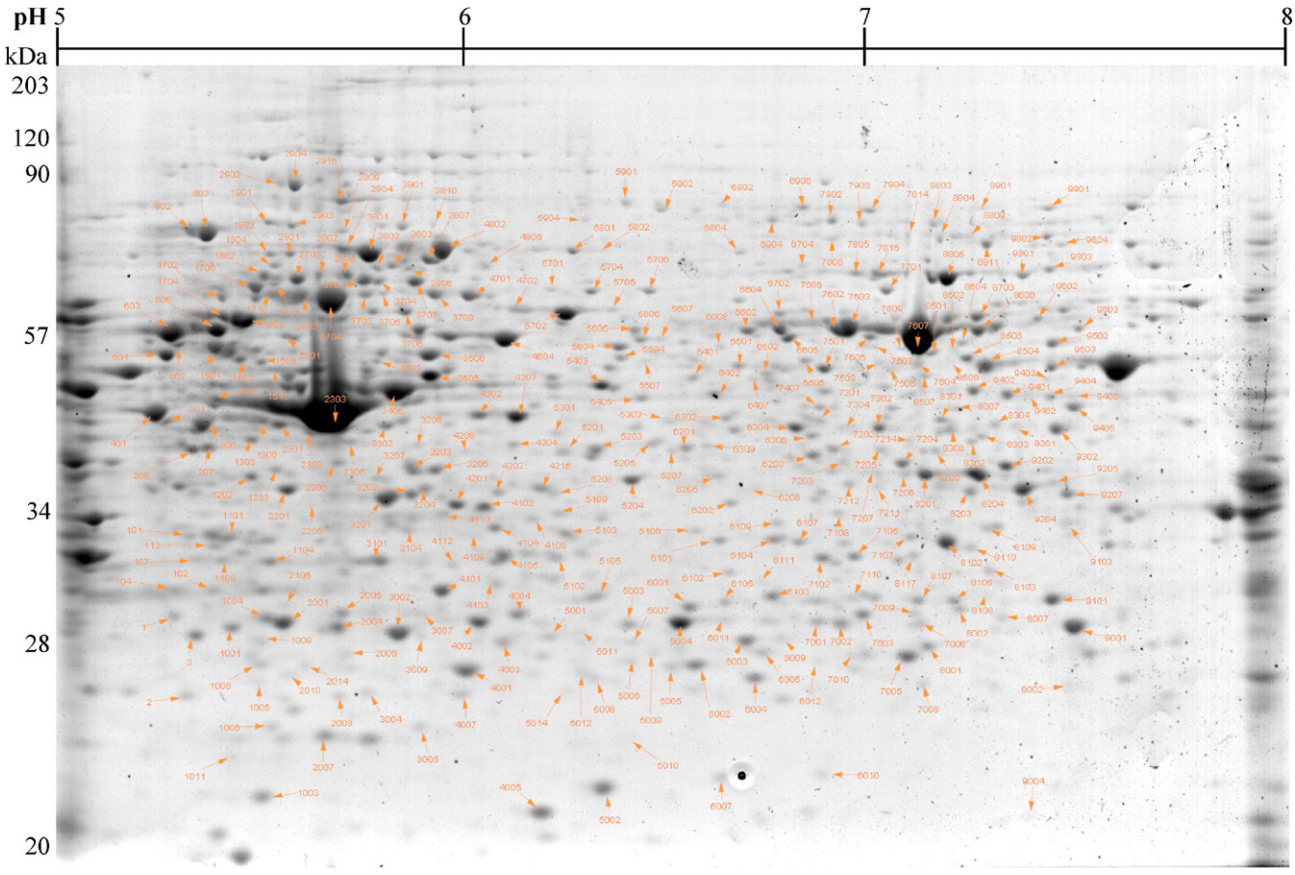

Fig. 3. 2D-GE map of proteins in A549 cells used for further protein identification by mass spectrometry. The numbers in the map correspond to the identified protein spots listed in Table 2 of the "Data in Brief" article [42] submitted along with this manuscript.

interaction was significant for a protein spot, its change in expression for a given treatment and dose that was found significant by Holm-Sidak analysis was reported as it is, as seen in Table 2. The same applied for those proteins that were found to have significant *Treatment* and *Dose* main effects. If a protein was found to have significant *Treatment* main effect, fold changes were estimated using least mean square [39,40]. In the case where the *Dose* main effect was significant, the average fold change estimate was reported for each significant dose group. It should be noted that multiple protein spots with the same protein ID may have a p-value < 0.05, which suggests different isoforms of the same protein were significantly altered, and thus rigorous assessment may be required for proper interpretation of biological implication if the directions of change of these isoforms are different. However, our data showed that the direction of expression of all significant protein spots with the same ID aligned in the same direction, thus we chose the protein with the greatest fold-change (either increase or decrease) to conduct pathway analysis. Protein interaction network and pathway analyses were conducted by Ingenuity Pathway Analysis (www.ingenuity.com). Venn diagrams used to assess the similarities and/or differences in the protein profile following particle exposures were generated *via* VENNY [41].

3. Results

3.1. Cytotoxic assays

Cellular LDH levels (Fig. 1A) were found to decrease with particle dose (Two-way ANOVA: *Dose* main effect, $p < 0.05$; Holm-Sidak: 140, 200 *vs* 0 μg/cm^2, $p < 0.05$). Reduction in cytoplasmic LDH was more pronounced after exposure to CB than with TiO_2, but this difference did not reach statistical significance. Cellular proliferation measured by BrdU incorporation (Fig. 1B) was decreased by exposure to CB, but not with TiO_2 (Fig. 1B; Two-way ANOVA, *Treatment* × *Dose* interaction, $p < 0.05$; Holm-Sidak: 60, 140, 200 vs 0 μg CB/cm^2, $p < 0.05$). Decrease of cellular ATP (Fig. 1C) was statistically significant for treatment (Two-way ANOVA, *Treatment* main effect, $p < 0.05$; Holm-Sidak: CB vs TiO_2, $p < 0.05$) and dose (Two-way ANOVA, *Dose* main effect, $p < 0.05$; Holm-Sidak: 200 vs 0 μg/cm^2, $p < 0.05$). Resazurin reduction assay (Fig. 1D) revealed a *Treatment* × *Dose* interaction (Two-way ANOVA: *Treatment* × *Dose*, $p < 0.05$; Holm-Sidak, 60, 140 & 200 vs 0 μg/cm^2, $p < 0.05$), where only CB, but not TiO_2, significantly increased the reduction of resazurin.

Table 1
Two-way ANOVA results for the A549 protein spot changes due to particle exposures (n = 3). The number below *Treatment* main effect (Trt), *Dose* main effect (Dose) or interaction (T × D) corresponds to the p-value, where the bold number is <0.05. The number below the particles corresponds to the adjusted fold change (versus control) of the protein. Only the protein spots identified by MALDI-TOF-TOF-MS are provided here.

		Two-way ANOVA			TiO_2 (μg/cm^2)			CB (μg/cm^2)		
SSP	Protein	Trt	Dose	T × D	60	140	200	60	140	200
3202	CAPZA1	**0.004**	**0.016**	**0.031**						1.15
9804	FUBP1	**0.039**	0.947	**0.044**			1.29			−1.41
7701	CCT6A	0.507	**0.031**	**0.034**						1.51
8501	EEF2	0.571	**0.004**	**0.020**		3.00				−2.63
6501	PA2G4	0.165	**0.023**	**0.047**						1.40
7501	PA2G4	0.953	**0.009**	**0.037**						1.49
1602	TUBA1C	0.793	**0.015**	**0.049**						2.43
2902	VCP	0.457	**0.002**	**0.024**						1.63
7603	ALDH1A1	0.096	0.131	**0.034**			−1.61			
6604	CCT2	0.792	0.237	**0.023**			−1.24			1.53
4702	PDIA3	0.368	0.220	**0.021**					1.45	
3207	TRIM28	0.192	0.096	**0.035**			1.49			−1.44
4102	VCP	0.554	0.083	**0.036**						−1.35
2006	CRK	<**0.001**	<**0.001**	0.085	1.29	1.77	1.44	4.28	6.20	5.93
8205	AKR1A1	**0.041**	0.431	0.395				1.33	1.33	1.33
102	HSPA5	**0.017**	0.134	0.441				1.51	1.51	1.51
8809	LMNA	**0.028**	0.311	0.303	−1.10	−1.10	−1.10	1.19	1.19	1.19
2301	TMOD3	**0.005**	0.201	0.139	−1.19	−1.19	−1.19	1.28	1.28	1.28
6502	ANXA7	0.124	**0.037**	0.502		1.32	−1.68		1.32	−1.68
8108	ARMCX1	0.472	**0.017**	0.379		1.88			1.88	
9502	DIS3L	0.298	**0.000**	0.504			−1.52			−1.52
8107	EEF2	0.580	**0.031**	0.719		1.52	−1.30		1.52	−1.30
7205	ENO1	0.723	**0.021**	0.416		1.59	−1.18		1.59	−1.18
8503	ENO1	0.413	**0.035**	0.561		1.32	−1.29		1.32	−1.29
9405	ENO1	0.876	**0.043**	0.593		1.57	−1.26		1.57	−1.26
5607	HNRNPH1	0.852	**0.022**	0.458		−1.33	1.35		−1.33	1.35
2701	HNRNPK	0.913	**0.020**	0.146		−1.77			−1.77	
3104	HSP90AB3P	0.568	**0.026**	0.615		1.56	−1.15		1.56	−1.15
8106	HSPA8	0.622	**0.035**	0.533		1.51	−1.07		1.51	−1.07
8117	IDH1	0.899	**0.014**	0.443		1.58	−1.37		1.58	−1.37
5902	IMMT	0.510	**0.019**	0.761	1.35	−1.38		1.35	−1.38	
3705	INA	0.967	**0.002**	0.084		2.16	1.72		2.16	1.72
8103	NIT2	0.410	**0.017**	0.797		1.26	−1.11		1.26	−1.11
8110	PDIA3	0.270	**0.029**	0.580		1.53	−2.30		1.53	−2.30
6306	PGK1	0.363	**0.034**	0.282		1.27	−1.43		1.27	−1.43
7204	PKM	0.431	**0.003**	0.922			−1.86			−1.86
8606	PKM	0.942	**0.026**	0.889			−1.68			−1.68
5105	PSMB7	0.367	**0.019**	0.466			1.38			1.38
8301	RBM4	0.676	**0.038**	0.402	1.65			1.65		
8308	RBM4	0.708	**0.025**	0.634		−1.27			−1.27	
2904	VCP	0.745	**0.004**	0.141		−2.23			−2.23	
5301	XXYLT1	0.131	**0.008**	0.499	1.24	1.19	1.26	1.24	1.19	1.26

3.2. Two-dimensional gel electrophoresis (2D-GE)

It was experimentally determined that approximately 200 μg of protein can be extracted from 1×10^6 A549 cells. The protein profile of the A549 cells was initially evaluated with two pH ranges (pH 3–10 and pH 5–8) in the first dimension, while keeping the second dimension constant (12% SDS-PAGE). The 2D gel image in Fig. 2A showed that the pH 3–10 range encompassed most of the proteins detected by Coomassie blue. The pH 5–8 range gel detected approximately 85% of the proteins that were found in the pH 3–10 range (Fig. 2B). The protein spots in the pH 5–8 range were notably better resolved than that of pH 3–10. For this reason, the pH 5–8 range and 12% SDS-PAGE were selected to examine changes in the proteome of A549 cells following particle exposure. It was determined that when using 11 cm, pH 5–8 IPG strips, the optimal protein loading to visualize Coomassie Blue stained protein spots was between 100 and 175 μg (data not shown), as lower protein amounts resulted in missing spots, and higher protein loading led to poor resolution between spots due to the limited separation capacity of the 11 cm IPG strip. Coomassie blue stain was chosen since it is economical for the purpose of large toxicity screening studies and it is also compatible with MALDI-TOF-TOF-MS.

To assess the A549 proteome differences due to particle exposures, a common area that clearly displayed the majority of protein spots was employed across all experimental gels (Fig. 2B). This area (between pH 5.1–7.8 and 20–100 kDa) was chosen to overcome the typical warping, distortion and variation that were commonly encountered with 2D gels, particularly near the extremities of the molecular weight and pH range. Of the 543 protein spots detected in the common area of the gels, 333 spots were identified with MALDI-TOF-TOF-MS/MS (Fig. 3 and Table 2 in the related "Data in Brief" article [42]). In many cases, the same protein was detected in multiple spots; these multiple IDs (likely representing post-translational modifications, isoforms or degradation products) are summarized in Table 2 in the related "Data in Brief" article. In total, the 2D-GE map resulted in the identification of 180 unique proteins.

3.3. PM-induced changes in the proteome of A549 cells

Analysis of proteomic changes due to particle exposures revealed that the expressions of 60 protein spots were affected by both TiO_2 and CB, of which 42 protein spots were identified by MALDI-TOF-TOF-MS (Table 1). For proteins represented by multiple spots, the spot with the greatest fold change was selected for pathway analysis as mentioned in the Materials and Methods. Particle dose-related changes were noticed in 24 protein spots (Two-way ANOVA: *Dose* main effect, $p < 0.05$), 20 of which are unique proteins. Particle type-specific changes were noticed in 5 protein spots (Two-way ANOVA: *Treatment* main effect, $p < 0.05$), all of which are unique proteins; while 13 protein spots exhibited *Treatment* × *Dose* interaction (Two-way ANOVA: *Treatment* × *Dose* main effect, $p < 0.05$), 12 of these are unique proteins. Fig. 4A illustrates the effect of TiO_2 and CB exposures on A549 cellular proteome, where the particles up- and down-regulated the expression of proteins. The proteins that were affected commonly by both particle exposures and particle-specific alteration are shown in Fig. 4B and C. Protein interaction network and pathway analyses revealed that all the proteins (common and unique) affected by the two particles were

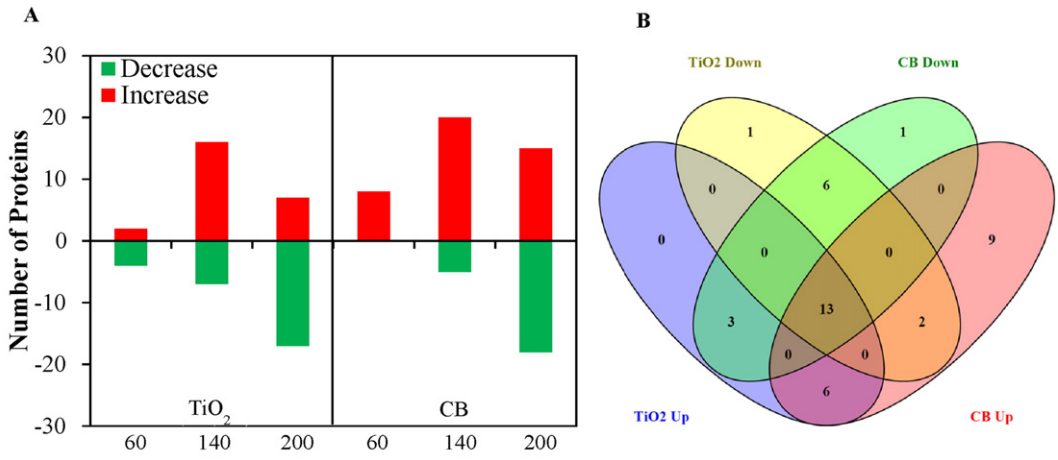

C

Only CB↑: 9		Only CB↓: 1		Only TiO_2↓: 1		CB↑ TiO_2↓: 2		CB↓ TiO_2↑: 3		CB↓ TiO_2↓: 6		CB↑ TiO_2↑: 6		CB↑ CB↓ TiO_2↑ TiO_2↓: 13	
SSP	Protein	SSP	Protein	SSP	Protein	SSP	Protein	SSP	Protein	SSP	Protein	SSP	Protein	SSP	Protein
102	HSPA5	4102	VCP	7603	ALDH1A1	2301	TMOD3	3207	TRIM28	2701	HNRNPK	8108	ARMCX1	6502	ANXA7
1602	TUBA1C					8809	LMNA	8501	EEF2	2904	VCP	2006	CRK	8107	EEF2
2902	VCP							9804	FUBP1	7204	PKM	3705	INA	7205	ENO1
3202	CAPZA1									8308	RBM4	5105	PSMB7	8503	ENO1
4702	PDIA3									8606	PKM	8301	RBM4	9405	ENO1
6501	PA2G4									9502	DIS3L	5301	XXYLT1	5607	HNRNPH1
7501	PA2G4													3104	HSP90AB3P
7701	CCT6A													8106	HSPA8
8205	AKR1A1													8117	IDH1
														5902	IMMT
														8103	NIT2
														8110	PDIA3
														6306	PGK1

Fig. 4. Two-way ANOVA results of differentially expressed proteins (p-value <0.05) in A549 cells following exposures to carbon black (CB) or titanium dioxide (TiO_2). (A) The bar graph shows the number of proteins which increased or decreased in expression following particle treatments at doses 60, 140 and 200 μg/cm^2. (B) The Venn diagram shows the number of proteins that exhibited specific and non-specific changes due to particle exposures. (C) Tabulation of unique and common proteins associated with CB and TiO_2 exposures. Only the proteins that were identified by MALDI-TOF-TOF-MS/MS are shown. ↑ indicates increased expression and ↓ specifies decreased expression.

Table 2
All A549 proteins that exhibited altered expressions (fold change compared to control) due to particle exposures and relevant cellular functions using Ingenuity Pathway Analysis.

Cellular	TiO_2 (μg/cm^2)			CB (μg/cm^2)		
Function	60	140	200	60	140	200
Cell death (apoptosis & necrosis)						
ALDH1A1			−1.61			
ANXA7		1.32	−1.68		1.32	−1.68
ENO1[a]		1.57	−1.26		1.57	−1.26
FUBP1			1.29			−1.41
CRK	1.29	1.77	1.44	4.28	6.20	5.93
HNRNPH1		−1.33	1.35		−1.33	1.35
HNRNPK		−1.77			−1.77	
HSPA5				1.51	1.51	1.51
HSPA8		1.51	−1.07		1.51	−1.07
IMMT	1.35	−1.38		1.35	−1.38	
LMNA	−1.10	−1.10	−1.10	1.19	1.19	1.19
PA2G4[a]						1.49
PDIA3[a]		1.53	−2.30		1.53	−2.30
PKM[a]			−1.86			−1.86
TMOD3	−1.19	−1.19	−1.19	1.28	1.28	1.28
TRIM28			1.49			−1.44
VCP[a]		−2.23			−2.23	1.63
CCT6A						1.51
CCT2			−1.24			1.53
Inflammation						
AKR1A1				1.33	1.33	1.33
ANXA7		1.32	−1.68		1.32	−1.68
EEF2[a]		3.00	−1.30		1.52	−2.63
ENO1[a]		1.57	−1.26		1.57	−1.26
FUBP1			1.29			−1.41
HSPA5				1.51	1.51	1.51
HSPA8		1.51	−1.07		1.51	−1.07
PDIA3[a]		1.53	−2.30		1.53	−2.30
PGK1		1.27	−1.43		1.27	−1.43
PKM[a]			−1.86			−1.86
TRIM28			1.49			−1.44
TUBA1C						2.43
VCP[a]		−2.23			−2.23	1.63
Protein metabolism						
CRK	1.29	1.77	1.44	4.28	6.20	5.93
EEF2[a]		3.00	−1.30		1.52	−2.63
HNRNPK		−1.77			−1.77	
HSPA5				1.51	1.51	1.51
PDIA3[a]		1.53	−2.30		1.53	−2.30
RBM4[a]	1.65	−1.27		1.65	−1.27	
VCP[a]		−2.23			−2.23	1.63
Cell survival & viability						
EEF2[a]		3.00	−1.30		1.52	−2.63
IDH1		1.58	−1.37		1.58	−1.37
LMNA	−1.10	−1.10	−1.10	1.19	1.19	1.19
PDIA3[a]		1.53	−2.30		1.53	−2.30
PKM[a]			−1.86			−1.86
TRIM28			1.49			−1.44
HSPA5				1.51	1.51	1.51
VCP[a]		−2.23			−2.23	1.63
Cell proliferation						
ANXA7		1.32	−1.68		1.32	−1.68
ENO1[a]		1.57	−1.26		1.57	−1.26
CRK	1.29	1.77	1.44	4.28	6.20	5.93
HNRNPK		−1.77			−1.77	
HSPA8		1.51	−1.07		1.51	−1.07
IDH1		1.58	−1.37		1.58	−1.37
IMMT	1.35	−1.38		1.35	−1.38	
LMNA	−1.10	−1.10	−1.10	1.19	1.19	1.19
PDIA3[a]		1.53	−2.30		1.53	−2.30
PGK1		1.27	−1.43		1.27	−1.43
VCP[a]		−2.23			−2.23	1.63
ALDH1A1			−1.61			
CCT2			−1.24			1.53
DIS3L			−1.52			−1.52
PKM[a]			−1.86			−1.86
TRIM28			1.49			−1.44
HSPA5				1.51	1.51	1.51
CAPZA1						1.15
PA2G4[a]						1.49

(continued on next page)

Table 2 (*continued*)

Cellular	TiO_2 (μg/cm^2)			CB (μg/cm^2)		
Function	60	140	200	60	140	200
Cell migration						
CRK	1.29	1.77	1.44	4.28	6.20	5.93
ENO1[a]		1.57	−1.26		1.57	−1.26
HNRNPK		−1.77			−1.77	
HSPA5				1.51	1.51	1.51
IDH1		1.58	−1.37		1.58	−1.37
LMNA	−1.10	−1.10	−1.10	1.19	1.19	1.19
PA2G4[a]						1.49
PDIA3[a]		1.53	−2.30		1.53	−2.30
PKM[a]			−1.86			−1.86
TMOD3	−1.19	−1.19	−1.19	1.28	1.28	1.28
TUBA1C						2.43
VCP[a]		−2.23			−2.23	1.63

[a] Protein represented by multiple spots. The spot with the highest fold change was used as mentioned in the Materials and Methods.

known to be associated with cell death (necrosis and/or apoptosis), proliferation, migration, protein metabolism, inflammation and survival/viability pathways (Table 2). To determine the toxicoproteomic differences between TiO_2 and CB, the proteins that were differentially affected by the two particles were interrogated; these proteins were highlighted in Table 1 that two-way ANOVA identified as significant for interaction and treatment main effects. The results in Table 3 show that the differential toxicoproteomic effect between TiO_2 and CB lies mainly in those proteins that regulate proliferation, viability, apoptosis and necrosis in cells. Fig. 5 shows that there were distinctive patterns of protein expression in A549 cells in response to the two particles as demonstrated in the networks of cell death (apoptosis and necrosis) and cell proliferation pathways.

4. Discussion

In this work, we utilized a well-established human lung epithelial cell line (A549) to assess the effects of CB and TiO_2, two respirable particles with distinct chemical and physical properties. Decrease of the cytoplasmic LDH content is suggestive of alteration of cell membrane integrity. BrdU incorporation, which assesses DNA synthesis during cell proliferation, was reduced with increasing doses of CB but not TiO_2. Cellular energy metabolism investigated by the ATP assay demonstrated that both particles reduced the level of ATP in A549 cells, with CB being more potent than TiO_2. In the resazurin reduction assay, CB but not TiO_2 increased the rate of reduction. In short, the results from the cytotoxicity assays indicate that A549 cells were reactive to the particles, with CB being more potent than TiO_2 in eliciting cellular responses, but both particles were mildly cytotoxic under the experimental conditions with a cellular viability greater than 75% at the highest exposure level tested.

Cellular proteomic changes were analyzed by 2D-GE followed by protein identification using mass spectrometry. We chose to examine the A549 proteome in the window of pH 5.2–pH 7.8 and 100–20 kDa because this area contained most of the protein spots (543) that were well-resolved across all experimental gels (Fig. 2B). Of the 543 protein spots, we have determined the identities of 333 protein spots *via* MALDI-TOF-TOF-MS/MS, and to our knowledge this is the largest repository of A549 cellular proteome identified by 2D-GE thus far. It should be noted that the same protein was detected in multiple spots in many cases (Table 2 in the related "Data in Brief" article [42]), where these multiple IDs are likely representing post-translational modifications, isoforms or degradation products of the same protein.

Two-way ANOVA revealed that 60 of the protein spots showed significant changes ($p < 0.05$) as *Treatment* or *Dose* main effects, and with *Treatment* × *Dose* interaction following exposure of cells to TiO_2 and CB (Table 1). Fig. 4A illustrates the effect of TiO_2 and CB exposures on A549 cellular proteome, where the particles up- and down-regulated the expression of proteins. This figure showed that 140 μg/cm^2 doses led to increased expression of more proteins relative to both 60 and 200 μg/cm^2 doses. These findings can potentially be attributed to non-monotonous toxicity effects. It is possible that the medium dose (140 μg/cm^2) enhanced protein synthesis as a response to increased toxicity compared to the low dose, whereas at the highest toxic dose (200 μg/cm^2), reduced protein synthesis and enhance protein degradation can occur as a result of cellular apoptosis.

It should be noted that the significant cut-off p-value was set at 0.05, it is possible that 27 significant spots (5% of 543 protein spots examined) could be false positive by random chance. However, proteins do not act on their own in a cell, they normally interact with one

Table 3
A549 proteins that are differentially affected by TiO_2 and CB and associated cellular functions. The proteins in this table were identified by two-way ANOVA as *Treatment* main effect and *Treatment* × *Dose* interaction, which were highlighted in Table 1.

Cellular	TiO_2 (μg/cm^2)			CB (μg/cm^2)		
Function	60	140	200	60	140	200
Cell death (*apoptosis* & *necrosis*)						
ALDH1A1			−1.61			
CCT2			−1.24			1.53
CCT6A						1.51
FUBP1			1.29			−1.41
CRK	1.29	1.77	1.44	4.28	6.20	5.93
HSPA5				1.51	1.51	1.51
LMNA	−1.10	−1.10	−1.10	1.19	1.19	1.19
PA2G4[a]						1.49
TMOD3	−1.19	−1.19	−1.19	1.28	1.28	1.28
TRIM28			1.49			−1.44
VCP[a]		−2.23			−2.23	1.63
Cell viability						
EEF2		3.00	−1.30		1.52	−2.63
HSPA5				1.51	1.51	1.51
LMNA	−1.10	−1.10	−1.10	1.19	1.19	1.19
TRIM28			1.49			−1.44
VCP[a]		−2.23			−2.23	1.63
Cell proliferation						
ALDH1A1			−1.61			
CAPZA1						1.15
CCT2			−1.24			1.53
CRK	1.29	1.77	1.44	4.28	6.20	5.93
HSPA5				1.51	1.51	1.51
LMNA	−1.10	−1.10	−1.10	1.19	1.19	1.19
PA2G4[a]						1.49
TRIM28			1.49			−1.44
VCP[a]		−2.23			−2.23	1.63

[a] Protein represented by multiple spots. The spot with the highest fold change was used as mentioned in the Materials and Methods.

another in a network or pathway to carry out a particular function. Thus, when a group of proteins in a particular pathway were identified as significantly altered with unadjusted p-value < 0.05, we posit that changes in a group of proteins are not likely to occur by random chance. Therefore, we decided to retain the 60 significant protein spots with p-value < 0.05 (not adjusted for false discovery), and the identities of 42 of these spots have been determined *via* MALDI-TOF-TOF-MS (Fig. 4 and Table 1). In pathway analysis, only those pathways that were influenced by >5 significant proteins in any treatment were flagged as possible pathways that were affected by exposure treatments.

Ingenuity pathway analysis revealed that TiO_2 and CB can significantly alter the expression of proteins that are known to be involved in inflammation, protein metabolism, cell migration, proliferation, death and survival (Table 2). Although the use of all significant proteins for pathway analysis gave an overall idea of the cellular functions that can be affected by both particles, in order to dissect the toxicoproteomic differences between TiO_2 and CB, we selected the proteins that were unique to TiO_2 and CB exposures for pathway analysis (Table 3). The results in Table 3 demonstrated that the proteins that regulate cell proliferation, viability, apoptosis and necrosis were affected by TiO_2 and CB differently. Nevertheless, the number of proteins that are unique to these pathways was found to be low. For instance, CCT6A, EEF2 and CAPZA1 were unique to cell death, cell viability and cell proliferation respectively, while the others were common to all three pathways. Even though it is possible that there can be network ambiguity through IPA analyses, the significant proteins that were affected by both particles in Table 2 showed more unique proteins specific to cell death (*e.g.*, CCT6A, FUBP1, HNRNPH1 and TMOD3) and cell proliferation (*e.g.*, CAPZA1, DIS3L and PGK1) pathways. In addition, the cytotoxicity assay results are indicative of induced cell death (decreased cellular LDH and ATP levels) and decreased cell proliferation (decreased BrdU incorporation) pathways upon particle exposures. Together, these

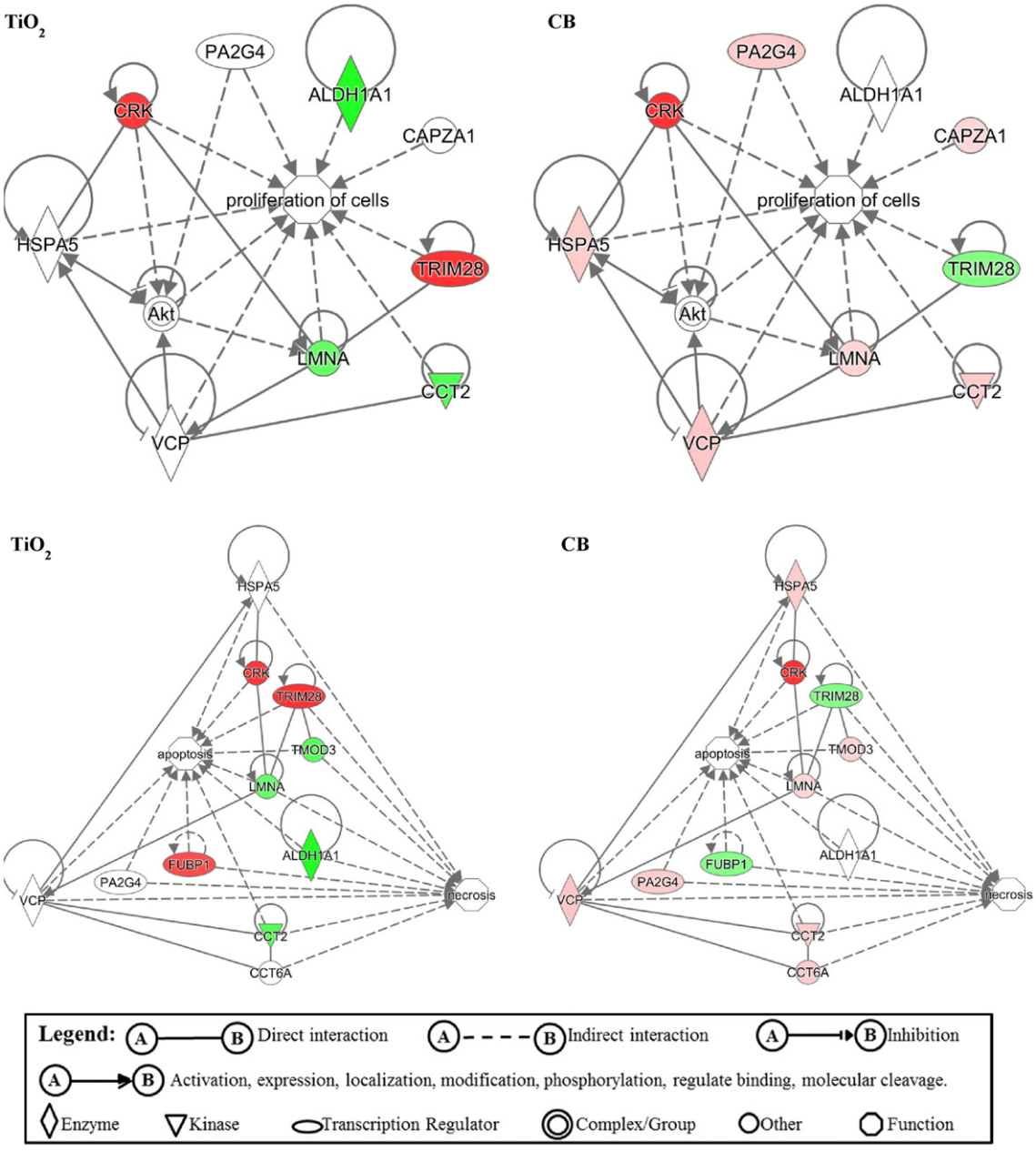

Fig. 5. The networks of cell death (apoptosis and necrosis) and cell proliferation pathways that emphasize the toxicoproteomic differences between TiO_2 and CB at the dose 200 μg/cm^2 (Table 3). Red is for increased expression and green is for decreased expression.

observations suggest that these particle exposures affected cell death, cell viability and cell proliferation pathways in the A549 cells.

The networks of protein-protein interaction in Fig. 5 showed how the two particles distinctively affected those proteins involved in cell death and proliferation pathway. In the network of cell proliferation, TiO_2 specifically increased the expression of TRIM28 and decreased the expression of ALDH1A1, CCT2 and LMNA, while CB specifically decreased the expression of TRIM28 and increased the expression of CAPZA1, CCT2, HSPA5, LMNA, PA2G4 and VCP. The serine/threonine kinase Akt is a well-recognized signaling hub that orchestrates various cellular functions (including cell growth and survival) and this protein interacts directly and indirectly with the majority of the proteins that were up-regulated only by CB treatments (Fig. 5). It would be interesting to examine the time-related functional interactions between Akt and these proteins. For example, the level of LMNA is reportedly regulated by the serine/threonine kinase Akt in C2C12 mouse myoblasts and HEK293 human embryonic kidney epithelial cells [43], where Akt can phosphorylate LMNA and targets it for degradation through a lysosomal mechanism [43], and Akt can also regulate the transcription of LMNA [43]. Since LMNA is an intermediate filament protein in the nuclear lamina that must be degraded for DNA synthesis and mitosis to occur, an increase in LMNA expression in A549 cells exposed to CB can be a marker of DNA synthesis, which was supported by BrdU incorporation assay (Fig. 1B). Another protein that interacts with Akt and affects the proliferation of cells is PA2G4 that can bind to the androgen receptor [44] and transcriptionally repress genes regulated by the receptor [45]. Overexpression of PA2G4 has been reported to inhibit growth in LNCaP human prostate adenocarcinoma cells [45], NIH3T3 human fibroblasts [46] and rat pheochromocytoma PC-12 cells [47]. Thus, the observed increased expression of PA2G4 in A549 mediated by CB exposure can be another marker that suppresses cell proliferation. In essence A549 cellular proteomic changes relevant to CB exposure involved in reduction in cell proliferation are consistent with the level of BrdU incorporation.

Toxicoproteomics also revealed particle-specific changes in the level and/or direction of a unique set of proteins that are known to regulate cell death (apoptosis and necrosis) (Table 3). In the protein-protein interaction network of the cell death pathway in Fig. 5, about a dozen of A549 proteins showed a stark difference between TiO_2 and CB exposures. For example, TiO_2 specifically increased the expression of TRIM28 and FUBP1 but decreased the expression of ALDH1A1, CCT2, LMNA and TMOD3. On the other hand, CB specifically decreased the expression of TRIM28 and FUBP1 but increased the expression of CAPZA1, CCT2, CCT6A, HSPA5, LMNA, PA2G4 and VCP. A number of these proteins can also be found in the cell proliferation network as these proteins have anti-proliferative effect as discussed above. Interestingly, CB appears to cause more cell death in A549 cells than TiO_2 based on the LDH assay (Fig. 1A), but the variance in this assay did not allow statistical analysis to differentiate the toxic potencies between the two particles. Thus, toxicoproteomics is more sensitive in distinguishing the subtle effect of the particles on the cell death pathways. In addition, the VCP ATPase [48] and HSPA5 heat shock protein [49] in the endoplasmic reticulum are associated with ATPase activity, and thus CB-induced increases in VCP and HSPA5 can lower the level of cellular ATP by enhancing ATPase activity in A549 cells. These findings were supported by ATP assay (Fig. 1C). In essence, the results of our study demonstrated that toxicoproteomics is a sensitive and informative method to differentiate the toxic effects of particulate matter.

5. Conclusion

In vitro toxicoproteomics has the capacity to distinguish cellular responses to two particles with distinct chemical and physical properties as illustrated by TiO_2 and CB exposures of A549 cells. The particles caused common and distinct A549 cellular responses that were detectable via cytotoxicity assays and high-content proteomic analysis, which can be useful to investigate the molecular mechanisms of particle toxicity. This toxicoproteomic approach can be valuable in future particle toxicity evaluation studies.

Acknowledgements

We would like to thank Drs. Errol Thomson and Bhaja Krushna Padhi for their helpful comments. This work was supported by the Clean Air Regulatory Agenda at Health Canada (HC4340565) and, Ontario Graduate Scholarship in Science and Technology (Student #1519592) and Ontario Graduate Scholarship (Student #1519592) (funding for Ngoc Vuong). We also acknowledge Christine MacKinnon-Roy and Alexandra Star for their valuable technical assistance.

References

[1] J.A. Scott, Fog and deaths in London, December 1952, Public Health Rep. 68 (5) (1953) 474–479.
[2] P. Stocks, Cancer and bronchitis mortality in relation to atmospheric deposit and smoke, Br. Med. J. 1 (5114) (1959) 74–79.
[3] L. Liu, L.Y. Yu, H.J. Mu, L.Y. Xing, Y.X. Li, G.W. Pan, Shape of concentration-response curves between long-term particulate matter exposure and morbidities of chronic bronchitis: a review of epidemiological evidence, J. Thorac. Dis. 6 (Suppl. 7) (2014) S720–S727.
[4] E.A. MacIntyre, M. Brauer, E. Melen, C.P. Bauer, M. Bauer, D. Berdel, et al., GSTP1 and TNF gene variants and associations between air pollution and incident childhood asthma: the traffic, asthma and genetics (TAG) study, Environ. Health Perspect. 122 (4) (2014) 418–424.
[5] M.W. Su, C.H. Tsai, K.Y. Tung, B.F. Hwang, P.H. Liang, B.L. Chiang, et al., GSTP1 is a hub gene for gene-air pollution interactions on childhood asthma, Allergy 68 (12) (2013) 1614–1617.
[6] C. Canova, C. Dunster, F.J. Kelly, C. Minelli, P.L. Shah, C. Caneja, et al., PM10-induced hospital admissions for asthma and chronic obstructive pulmonary disease: the modifying effect of individual characteristics, Epidemiology 23 (4) (2012) 607–615.
[7] P.C. Goeminne, M. Kicinski, F. Vermeulen, F. Fierens, B.K. De, B. Nemery, et al., Impact of air pollution on cystic fibrosis pulmonary exacerbations: a case-crossover analysis, Chest 143 (4) (2013) 946–954.
[8] S.C. Farhat, M.B. Almeida, L.V. Silva-Filho, J. Farhat, J.C. Rodrigues, A.L. Braga, Ozone is associated with an increased risk of respiratory exacerbations in patients with cystic fibrosis, Chest 144 (4) (2013) 1186–1192.
[9] F. Merlo, M. Costantini, G. Reggiardo, M. Ceppi, R. Puntoni, Lung cancer risk among refractory brick workers exposed to crystalline silica: a retrospective cohort study, Epidemiology 2 (4) (1991) 299–305.
[10] C.A. Pope III, R.T. Burnett, M.C. Turner, A. Cohen, D. Krewski, M. Jerrett, et al., Lung cancer and cardiovascular disease mortality associated with ambient air pollution and cigarette smoke: shape of the exposure-response relationships, Environ. Health Perspect. 119 (11) (2011) 1616–1621.
[11] J. Siemiatycki, R. Dewar, R. Lakhani, L. Nadon, L. Richardson, M. Gerin, Cancer risks associated with 10 inorganic dusts: results from a case-control study in Montreal, Am. J. Ind. Med. 16 (5) (1989) 547–567.
[12] L. Kachuri, P.J. Villeneuve, M.E. Parent, K.C. Johnson, S.A. Harris, Occupational exposure to crystalline silica and the risk of lung cancer in Canadian men, Int. J. Cancer (2013).
[13] M.J. Wang, C.A. Gray, S.A. Reznek, K. Mahmud, Y. Kutsovsky. Carbon black 4, 761–803. 03. Kirk-Othmer Encyclopedia of Chemical Technology (Generic).
[14] A.Y. Watson, P.A. Valberg, Carbon black and soot: two different substances, AIHAJ 62 (2) (2001) 218–228.
[15] C.M. Long, M.A. Nascarella, P.A. Valberg, Carbon black vs. black carbon and other airborne materials containing elemental carbon: physical and chemical distinctions, Environ. Pollut. 181 (2013) 271–286.
[16] M.L. Bell, Assessment of the health impacts of particulate matter characteristics, Res. Rep. Health Eff. Inst. 161 (2012) 5–38.
[17] J.I. Levy, D. Diez, Y. Dou, C.D. Barr, F. Dominici, A meta-analysis and multisite time-series analysis of the differential toxicity of major fine particulate matter constituents, Am. J. Epidemiol. 175 (11) (2012) 1091–1099.
[18] A. Schneider, R. Hampel, A. Ibald-Mulli, W. Zareba, G. Schmidt, R. Schneider, et al., Changes in deceleration capacity of heart rate and heart rate variability induced by ambient air pollution in individuals with coronary artery disease, Part. Fibre Toxicol. 7 (2010) 29.
[19] J.G. Wagner, A.S. Kamal, M. Morishita, J.T. Dvonch, J.R. Harkema, Rohr AC, PM2.5-induced cardiovascular dysregulation in rats is associated with elemental carbon and temperature-resolved carbon subfractions, Part. Fibre Toxicol. 11 (2014) 25.
[20] J.G. Lee, W.J. Noh, H. Kim, M.Y. Lee, Generation of reactive oxygen species contributes to the development of carbon black cytotoxicity to vascular cells, Toxicol. Res. 27 (3) (2011) 161–166.
[21] R.M. Mroz, R.P. Schins, H. Li, E.M. Drost, W. Macnee, K. Donaldson, Nanoparticle carbon black driven DNA damage induces growth arrest and AP-1 and NFkappaB DNA binding in lung epithelial A549 cell line, J. Physiol. Pharmacol. 58 (Suppl. 5(Pt 2)) (2007) 461–470.
[22] D. Sahu, G.M. Kannan, R. Vijayaraghavan, Carbon black particle exhibits size dependent toxicity in human monocytes, Int. J. Inflamm. 2014 (2014) 827019.

[23] D. Saputra, J.H. Yoon, H. Park, Y. Heo, H. Yang, E.J. Lee, et al., Inhalation of carbon black nanoparticles aggravates pulmonary inflammation in mice, Toxicol. Res. 30 (2) (2014) 83–90.
[24] H. Yamawaki, N. Iwai, Mechanisms underlying nano-sized air-pollution-mediated progression of atherosclerosis: carbon black causes cytotoxic injury/inflammation and inhibits cell growth in vascular endothelial cells, Circ. J. 70 (1) (2006) 129–140.
[25] R. Zhang, Y. Dai, X. Zhang, Y. Niu, T. Meng, Y. Li, et al., Reduced pulmonary function and increased pro-inflammatory cytokines in nanoscale carbon black-exposed workers, Part. Fibre Toxicol. 11 (1) (2014) 73.
[26] H.J. Johnston, G.R. Hutchison, F.M. Christensen, S. Peters, S. Hankin, V. Stone, Identification of the mechanisms that drive the toxicity of TiO(2) particulates: the contribution of physicochemical characteristics, Part. Fibre Toxicol. 6 (2009) 33.
[27] Y. Ge, M. Bruno, K. Wallace, S. Leavitt, D. Andrews, M.A. Spassova, et al., Systematic proteomic approach to characterize the impacts of chemical interactions on protein and cytotoxicity responses to metal mixture exposures, J. Proteome Res. 14 (1) (2015) 183–192.
[28] P. Kumarathasan, D. Das, M.A. Salam, S. Mohottalage, N. DeSilva, B. Simard, et al., Mass spectrometry-based proteomic assessment of the in vitro toxicity of carbon nanotubes, Curr. Top. Biochemica Res. 14 (1) (2012) 15–27.
[29] Y. Ge, M. Bruno, K. Wallace, W. Winnik, R.Y. Prasad, Proteome profiling reveals potential toxicity and detoxification pathways following exposure of BEAS-2B cells to engineered nanoparticle titanium dioxide, Proteomics 11 (12) (2011) 2406–2422.
[30] F. Hosp, R.A. Scheltema, C. Eberl, N.A. Kulak, E.C. Keilhauer, K. Mayr, et al., A double-barrel LC-MS/MS system to quantify 96 interactomes per day, Mol. Cell. Proteomics (2015).
[31] V. Malard, O. Prat, E. Darrouzet, F. Berenguer, N. Sage, E. Quemeneur, Proteomic analysis of the response of human lung cells to uranium, Proteomics 5 (17) (2005) 4568–4580.
[32] N. Morbt, J. Tomm, R. Feltens, I. Mogel, S. Kalkhof, K. Murugesan, et al., Chlorinated benzenes cause concomitantly oxidative stress and induction of apoptotic markers in lung epithelial cells (A549) at nonacute toxic concentrations, J. Proteome Res. 10 (2) (2011) 363–378.
[33] Y. Peng, Z.R. Gregorich, S.G. Valeja, H. Zhang, W. Cai, Y.C. Chen, et al., Top–down proteomics reveals concerted reductions in myofilament and Z-disc protein phosphorylation after acute myocardial infarction, Mol. Cell. Proteomics 13 (10) (2014) 2752–2764.
[34] X. Yang, J. Liu, H. He, L. Zhou, C. Gong, X. Wang, et al., SiO2 nanoparticles induce cytotoxicity and protein expression alteration in HaCaT cells, Part. Fibre Toxicol. 7 (2010) 1.
[35] R. Vincent, P. Goegan, G. Johnson, J.R. Brook, P. Kumarathasan, L. Bouthillier, et al., Regulation of promoter-CAT stress genes in HepG2 cells by suspensions of particles from ambient air, Fundam. Appl. Toxicol. 39 (1) (1997) 18–32.
[36] D. Nadeau, R. Vincent, P. Kumarathasan, J. Brook, A. Dufresne, Cytotoxicity of ambient air particles to rat lung macrophages: comparison of cellular and functional assays, Toxicol. in Vitro 10 (2) (1996) 161–172.
[37] P. Kumarathasan, D. Breznan, D. Das, M.A. Salam, Y. Siddiqui, C. Mackinnon-Roy, et al., Cytotoxicity of carbon nanotube variants: a comparative in vitro exposure study with A549 epithelial and J774 macrophage cells, Nanotoxicology (2014).
[38] P. Kumarathasan, S. Mohottalage, P. Goegan, R. Vincent, An optimized protein in-gel digest method for reliable proteome characterization by MALDI-TOF-MS analysis, Anal. Biochem. 346 (1) (2005) 85–89.
[39] S.R. Searle, F.M. Speed, G.A. Miliken, The population marginal means in the linear model: an alternative to least squares means, Am. Stat. 34 (1980) 216–221.
[40] J.H. Goodnight, W.R. Harvey, Least-squares means in the fixed-effects general linear models, SAS Institute Inc.: SAS Technical Report, Report No.: SAS Technical Report R-103, 1978.
[41] J.C. Oliveros. VENNY. An Interactive Tool for Comparing Lists With Venn's Diagrams. 15. http://bioinfogp.cnb.csic.es/tools/venny/index.html (Online Source).
[42] N.Q. Vuong, P. Goegan, S. Mohottalage, D. Breznan, M. Ariganello, A. Williams, et al., Human Lung Epithelial Cell Proteome Characterized by 2D-GE and MALDI-TOF-TOF-MS: Effect of Titanium Dioxide and Carbon Black Exposures. (Data in Brief 2016; Submitted on March 11, 2016).
[43] J. Bertacchini, F. Beretti, V. Cenni, M. Guida, F. Gibellini, L. Mediani, et al., The protein kinase Akt/PKB regulates both prelamin A degradation and Lmna gene expression, FASEB J. 27 (6) (2013) 2145–2155.
[44] Y. Zhang, J.D. Fondell, Q. Wang, X. Xia, A. Cheng, M.L. Lu, et al., Repression of androgen receptor mediated transcription by the ErbB-3 binding protein, Ebp1, Oncogene 21 (36) (2002) 5609–5618.
[45] Y. Zhang, X.W. Wang, D. Jelovac, T. Nakanishi, M.H. Yu, D. Akinmade, et al., The ErbB3-binding protein Ebp1 suppresses androgen receptor-mediated gene transcription and tumorigenesis of prostate cancer cells, Proc. Natl. Acad. Sci. U. S. A. 102 (28) (2005) 9890–9895.
[46] M. Squatrito, M. Mancino, M. Donzelli, L.B. Areces, G.F. Draetta, EBP1 is a nucleolar growth-regulating protein that is part of pre-ribosomal ribonucleoprotein complexes, Oncogene 23 (25) (2004) 4454–4465.
[47] Z. Liu, J.Y. Ahn, X. Liu, K. Ye, Ebp1 isoforms distinctively regulate cell survival and differentiation, Proc. Natl. Acad. Sci. U. S. A. 103 (29) (2006) 10917–10922.
[48] C. Song, Q. Wang, C.C. Li, ATPase activity of p97-valosin-containing protein (VCP). D2 mediates the major enzyme activity, and D1 contributes to the heat-induced activity, J. Biol. Chem. 278 (6) (2003) 3648–3655.
[49] M. Wisniewska, T. Karlberg, L. Lehtio, I. Johansson, T. Kotenyova, M. Moche, et al., Crystal structures of the ATPase domains of four human Hsp70 isoforms: HSPA1L/Hsp70-hom, HSPA2/Hsp70-2, HSPA6/Hsp70B', and HSPA5/BiP/GRP78, PLoS One 5 (1) (2010), e8625.